

N₂ TRANSFER AND CRITICAL PRESSURES IN TISSUE COMPARTMENTS

B. R. WIENKE

Applied Theoretical Physics Division, Los Alamos National Laboratory, Los Alamos, NM 87545, U.S.A.

(Received April 1986; accepted for publication February 1988)

Communicated by X. J. R. Avula

Abstract—Transfer mechanisms and critical pressures are essential elements in decompression calculations and staged procedures. By coupling a multi-tissue transfer model to fitted critical pressures, decompression data can be synthesized for rapid numerical implementation in air diving applications and procedures. Parametric fits to the critical N₂ pressures used to construct the U.S. Navy air tables are generated for the six tissue compartments (5, 10, 20, 40, 80 and 120 min) at sea level, with both linear and constant pressure ratio extrapolations to altitude conveniently effected with the barometer equation. The macroscopic model used to transfer inert N₂ in tissues is described and functional forms of the fit equations are motivated. Accurate (single parameter) exponential representations for mantle pressures, and the well-known Cross altitude factors, are also generated. Fitted critical tensions vary inversely as the approximate fourth root of the tissue half-life and increase linearly with depth. Air mantle pressures decrease exponentially with altitude and inverse temperature. Using bounce dive constraints, a set of bulk (single tissue) decay coefficients, which increase logarithmically with depth, are extracted from a Royal Navy (depth-dependent) decompression criteria and contrasted with corresponding multi-tissue decay parameters. Bends statistics and a decompression titration experiment, which predicts decreasing critical ratios at depth, are discussed. Overlapping predictions of the multi-tissue and bulk models, and correlations with experiment are identified.

I. INTRODUCTION

Calculations of decompression schedules for diving at sea level are based on a model originally used by the English physiologist J. S. Haldane [1]. His original observation, using experimental goats which had been chamber saturated to depths up to 165 feet of sea water (ft-sw) suggested the animals did not develop decompression sickness if subsequent decompression was limited to no greater than halving the ambient pressure. Thus animals saturated at 6 atm (absolute pressure) could be immediately decompressed to 3 atm, from 2 to 1 atm, and so forth. In all cases the critical saturation ratio (absolute N₂ pressure/absolute ambient pressure) was found to be 1.58, since the N₂ air fraction is 0.79. Translated to humans directly, researchers reckoned that body tissues and fluids apparently tolerate a 1.58 overpressure factor before the onset of decompression sickness, presumably because N₂ bubbles are not formed. Using these findings, Haldane then constructed decompression schedules which did not allow the critical saturation ratio of 1.58 to be exceeded in any of five theoretical tissue compartments. The tissue compartments were characterized by their half-life, i.e. the time required for the compartment to lose or gain 50% of existent N₂. The five original compartments (5, 10, 20, 40 and 75 min) were employed in decompression calculations and staged procedures [2] for 50 years with little modification.

In the mid-1950s, by empirically performing deep bounce dives and expanding the range of depths and exposures covered by the tables, the U.S. Navy advocated the use of six tissues (5, 10, 20, 40, 80, 120 min) in constructing decompression schedules, with each tissue compartment having its own critical ratio [3-7]. Temporal uptake and elimination of inert gas were based on a simple tissue response function [8] which addressed only the macroscopic aspects of N₂ transport in body tissues and fluids. Exact bubble production mechanisms, interplay of competing pressures and temperatures and related transport phenomenon were not quantified and remain only partially understood today, though pertinent research continues.

The interpretation given to the extensive body of experimental decompression data has also changed over the years. While Haldane and coworkers regarded critical ratios and pressures as limit points, separating bubble formation from non-bubble formation, the decompression data is more

properly a statistical predictor of bends thresholds for a given set of predisposing conditions. Decompression tables and procedures, as extracted from *experiment* and parameterized with *any* transfer model, serve to separate bends provoking exposures from non-bends provoking exposures within statistical confidence levels. In the same sense, bubble formation can then be viewed as symptomatic or sub-symptomatic, instead of present or non-present. Of course, fit equations, transfer models and biological response functions then gain efficacy by their ability to adequately reproduce experimental data, somewhat independent of their physical interpretation.

Inert N₂ transport in the body of a diver breathing compressed air is governed by many factors, such as gas diffusion, blood perfusion, phase separation, nucleation and cavitation, membrane permeation, fluid shifts and combinations thereof. Owing to the complexity of biological systems, multiplicity of tissues and media and diversity of boundary conditions, it is difficult to solve the N₂ transport problem directly in divers. Nonetheless, extensive efforts [9–13], over the past 75 years, directed toward establishment of safe diving procedures and formats, consistent with tests and measurements, have produced an empirical body of data called the decompression tables. Central to all tables are estimates of maximum N₂ saturation pressures, critical saturation or critical pressure differences and a tissue response function. We collect and quantify an extensive body of decompression data, and then fold this data over a response function which has been historically employed in decompression calculations and gross transfer modeling.

Specifically, a parametric fit to the critical pressures is described, with extrapolation to altitude using the barometer equation. Standard transport and decompression phenomenology are briefly reviewed. Linear and exponential treatments of atmospheric pressure are contrasted. A continuous representation for altitude pressure and Cross factors is detailed. Both linear and constant pressure ratio altitude extrapolations are discussed. Bulk coefficients are suggested, using bounce data and the Royal Navy critical ratios, and contrasted with the U.S. Navy multi-tissue parameters. Some statistics of bends occurrence and a simple, yet powerful, decompression titration experiment having interesting implications for critical ratios are briefly reviewed. Correlations between the two tissue models and experiment are discussed.

2. N₂ TRANSPORT AND DECOMPRESSION PHENOMENOLOGY

Transport of matter by random molecular motion across regions of varying concentration or, equivalently by Henry's law, pressure can be driven by the local gradient [8]. The classical approaches to decompression rest on this assumption. For a uniform system, the time rate of change of inert gas tissue tension is proportional to the difference between inspired partial pressure of the gas, p_i , and the instantaneous value, p ,

$$\frac{\partial p}{\partial t} = -\lambda(p - p_i), \quad (1)$$

with λ being the particular tissue decay parameter. Integrating equation (1), taking, $p = p_0$ at $t = 0$, yields

$$p - p_i = (p_0 - p_i)\exp(-\lambda t). \quad (2)$$

Similar gradient-driven linear phenomena, such as radioactive decay, reactive current flow, bulk heating and cooling, explosive burn propagation and signal attenuation, employ expressions closely resembling equation (2). The above equations have received the misnomer, *diffusion*, from investigators, probably because of semblance to transient heat flow expressions. Actually, equations (1) and (2) are simple rate equations, neither collisionally dominated diffusion nor streaming transport equations, and *bulk transfer* is more appropriate.

The time for $p - p_i$ to decrease to half its immediate value, after reduction in p_i , is the tissue half-life, τ . Six compartments with 5, 10, 20, 40, 80 and 120 min half-lives are generally employed in applications and half-lives are assumed to be independent of p_i . A one-to-one correspondence between the six compartments and specific anatomical entities is neither established, nor implied. Specification of the tissue half-life, τ permits immediate evaluation of the tissue decay constant,

λ , from equation (2),

$$\lambda = \frac{\ln 2}{\tau}. \quad (3)$$

Bulk, or single tissue, treatments [3] of N₂ transport, do not link λ to a particular compartment and are employed in bounce diving applications. Bulk decay constants may differ from the tissue constants given by equation (2) in attempting to account for the collective response of dominant compartments.

An underlying assumption built into equations (1)–(3) requires that blood saturated at ambient pressure will equilibrate with tissue at each round of circulation. Although one appreciates that the distribution of blood flow throughout the body is not uniform, so that better perfused tissues saturate faster than poorly perfused tissues, the continuous spectrum of perfusion-controlled response times is thus approximated by six compartments with time constants differing in roughly constant ratio. In this way, some perfusion limiting is implicit in the multi-tissue model. Intercellular spatial diffusion of inert gas occurs rapidly [11, 12] within circulation cycles, so as to not significantly limit, nor effect, the foregoing multi-tissue gradients.

If diffusion, perfusion and metabolic assimilation are mechanistically included, equation (1) generalizes to the Fick–Fourier expression,

$$\frac{\partial p}{\partial t} = \nabla \cdot D \nabla p - \kappa(p - p_i) - Z, \quad (4)$$

with ∇ the spatial gradient operator, D the diffusion coefficient, Z the metabolic consumption rate and κ a perfusion time constant, related to the perfusion rate, Γ , and partition fraction of gas (blood and tissue), v , by

$$\kappa = \Gamma v. \quad (5)$$

For inert gases, $Z = 0$, and we obviously take $D \approx 0$, with $\kappa = \ln 2/\tau$ in the multi-tissue sense. Additionally, discrepancies between measured values of D and those values needed to fit the decompression data exist [11, 12].

Denoting the ambient (absolute) pressure by P , Haldanian theory [1] assumes that the degree to which any tissue compartment tolerates N₂ supersaturation is limited by a critical ratio, r ,

$$\frac{p}{P} \leq r. \quad (6)$$

According to fixed gradient theory [2], tissue supersaturation is limited by a critical difference, l , such that

$$p - P \leq l. \quad (7)$$

Obviously r and l depend on many factors, not always discernible. The values of p for which the equalities hold in equations (6) and (7) are the critical tissue pressures, M , (*maximum values*). Determinations of r and l , or the corresponding critical pressures, M , have been a phenomenological thrust of decompression theory and bases for construction of staged decompression tables [9–13]. Early analyses employed fixed values for r , l and M , but today critical parameters generally vary across compartments, and with depth. Supersaturation theories regard the critical parameters as trigger points for bubble formation, while phase equilibration approaches treat the critical parameters as metastable limits for suspended gas transformation.

Uptake and elimination symmetry of the tissue response function, equation (3), remains valid only if the biological system maintains a true state of thermodynamic supersaturation and there is no separation of gas from solution. If inert gas separates (as it inevitably does according to nucleation theory [14]), the driving force for elimination can differ significantly from the uptake gradient, destroying the symmetry. The classical supersaturation assumptions are tantamount to a *bubble-free* hypothesis, but the presence (or non-presence) of bubbles does not affect the computational model, since expressions ultimately link to experimental values of r , l or M . However, for the record, the preponderance of measurement and theory [11, 12, 14] soundly

supports notions of nucleation, gas separation and bubble growth, even below observable bends thresholds.

Physical analyses of decompression focus directly on the microphysics of nucleation and bubble siting, gas separation, rate limiting effects and other biophysical influences to predict, or correlate, r , l and M from first principles [10–12, 14]. The empirical description, by focusing on the body of macroscopic data which has been gathered over the years, uses only coarse models to quantify the transfer mechanisms. Such a description is aptly a phenomenological approach.

3. EXPONENTIAL ATMOSPHERE AND BAROMETER EQUATION

Measuring pressure in feet of seawater (ft-sw) the absolute pressure, P , at depth, x , is given by

$$P = P_0 + x, \quad (8)$$

for surface atmospheric pressure, P_0 . At sea level, $P_0 = 33$ ft-sw. Above sea level, P_0 varies exponentially with altitude following a barometer equation. At approx. 18,000 ft, P_0 is half its value at sea level.

If air were an incompressible media, such as water, a simple linear dependence on altitude could be employed to compute P_0 . Since air is compressible, simple linear relationships such as those used compute water pressure are not generally applicable (though a simple linear reduction of P_0 with altitude is not a bad approximation over a low range of altitudes, as will be shown). Kinetic theory [15], which predicts the behavior of an ideal gas in a gravitational field, can be employed to compute P_0 . Assuming the constituent molecules of air are Maxwellian distributed (locally) at temperature, T , the total surface pressure, P_0 , at altitude, z , is obtained by summing the appropriate barometer expressions [15, 16] for each partial component (N_2 , O_2 and Ar) normalized to sea level pressure [16],

$$P_0 = 33 \sum_{n=1}^3 \alpha_n \exp(-\beta_n z/T), \quad (9)$$

with α_n the gas mixture fractions, β_n constants and temperature, T , measured in absolute (K) degrees. The three exponential (barometer) terms are the contributions of each component. Assuming a standard mixture of N_2 , O_2 and Ar, the partial fractions are simply [16]

$$\alpha_{N_2} = 0.7811, \quad \alpha_{O_2} = 0.2095, \quad \alpha_{Ar} = 0.0094, \quad (10)$$

and equation (9) thus represents an effective barometer equation for air. The factors β_n depend on the masses of the component gases, m_n , the acceleration of gravity, g , and Boltzmann's gas constant, k , according to

$$\beta_n = m_n g / k, \quad (11)$$

with specific values (K/ft)

$$\beta_{N_2} = 0.010067, \quad \beta_{O_2} = 0.011496, \quad \beta_{Ar} = 0.014361. \quad (12)$$

Variable concentrations of CO_2 and water vapor, and trace concentrations of heavier gases are neglected.

The comparative behavior of P_0 with altitude and temperature is shown in Fig. 1, which plots atmospheric pressure in increments of 1000 ft for Kelvin temperatures of 100, 300 and 500 K, (or -279 , 80 and $440^\circ F$). Departures from linear fall off are seen with both increasing altitude and decreasing temperature. Above roughly 7000 ft, linear extrapolations become less accurate for temperature ranges encountered on the earth.

The behavior of P_0 is also important to altitude diving modifications [17–24], especially the coupling to decompression criteria. Obviously, as $z \rightarrow \infty$ or $T \rightarrow 0$, we have $P_0 \rightarrow 0$ from equation (9), consistent with boundary conditions and thermodynamics. As $T \rightarrow \infty$, the atmosphere tends toward isotropy and P_0 decays very weakly with altitude. Over finite altitudes and less severe temperatures, a more complicated dependence is exhibited. Defining γ_n for convenience,

$$\lambda_n = \beta_n / T, \quad (13)$$

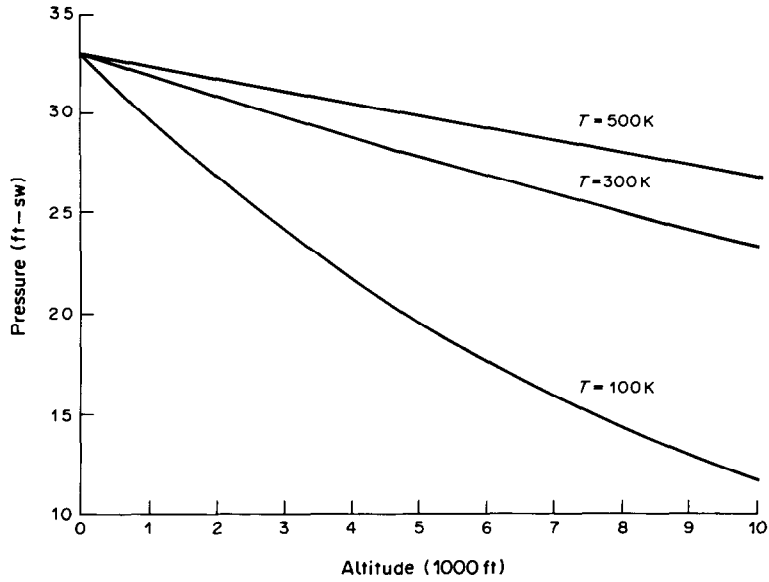


Fig. 1. Atmospheric pressure at altitude for different temperatures.

the exponential terms can be expanded in a Taylor series for $\gamma_n z < 1$:

$$\exp(-\gamma_n z) \approx 1 - \gamma_n z + \frac{1}{2}(\gamma_n z)^2. \tag{14}$$

Keeping only terms through first order from equation (14) and using equations (10) and (11), equation (9) reduces to a linear approximation for $\gamma_n z < 1$:

$$P_0 \approx 33[1 - (\alpha_{N_2}\gamma_{N_2} + \alpha_{O_2}\gamma_{O_2} + \alpha_{Ar}\gamma_{Ar})z]. \tag{15}$$

Relative accuracy depends on each $\gamma_n z$, and necessarily increases for high temperature and low altitudes. Similarly, the approximation is better for lighter gases than heavier gases, since β_n is directly proportional to the molecular mass.

Direct altitude measurements [25] of the earth's pressure mantle correlate with the barometer equation. Figure 2 contrasts measured pressures with equation (9) for $T = 273$ K (32°F). Seasonal and geographical variations of 7% are normal. Agreement between predicted and actual pressures is excellent (near 1% for altitudes up to 20,000 ft). Thus, taking $T = 273$ K in equation (13) gives

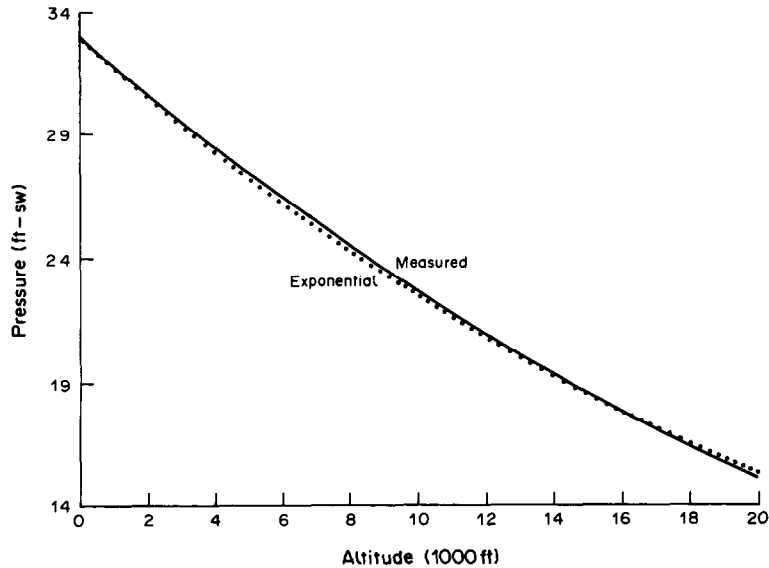


Fig. 2. Measured vs exponential atmospheric pressure at $T = 273$ K.

Table 1. Atmospheric pressure at altitude and cross factors.

Altitude (ft)	Pressure (ft-sw)	Cross factors
0	33.00	1.000
3000	29.57	1.116
6000	26.43	1.248
9000	23.60	1.399
12000	20.99	1.572
15000	18.65	1.770
18000	16.50	2.000

a good global estimate of atmospheric pressure, i.e.

$$\gamma_{N_2} = 0.000036875, \quad \gamma_{O_2} = 0.000042110, \quad \gamma_{Ar} = 0.000052604. \quad (16)$$

in units of ft^{-1} . Table 1 also lists atmospheric pressures in 3000-ft increments, up to 18,000 ft as well as the ratios of sea level pressure to altitude pressure, ξ ,

$$\xi = \frac{33}{P_0}, \quad (17)$$

which are the usual Cross (correction) factors [17, 20, 21] for altitude table conversion. Since P_0 decreases exponentially, clearly the Cross factors increase exponentially with altitude.

4. CRITICAL RATIOS AND N_2 PRESSURES

The critical pressures (M -values) collected by Des Granges [4] and Dwyer [7] for the tissue compartments at various depths, as well as the later compilation of Workman [6], represent a database for information reduction and extraction. Critical ratios [4], r , vs depth, x , are plotted in Fig. 3 (—) for the six tissue compartments at sea level, ($P_0 = 33$ ft-sw). Surfacing ratios [11], r_0 , and critical N_2 pressures, $M_0 = r_0 P_0$, are given in Table 2.

In general, U.S. Navy investigators claim that the overall incidence of decompression sickness is less than 1% in their data tabulations. While this is a genuine statistic, their figures include many no-stop exposures. When gradual (stage) decompression is required, Navy divers tend to be more conservative than the tables, effectively adding 5 or 10 min to their bottom time. Such procedure obviously renders the U.S. Navy statistics under predictive. A 5–10% bends incidence is probably more realistic [11, 12] using the above data.

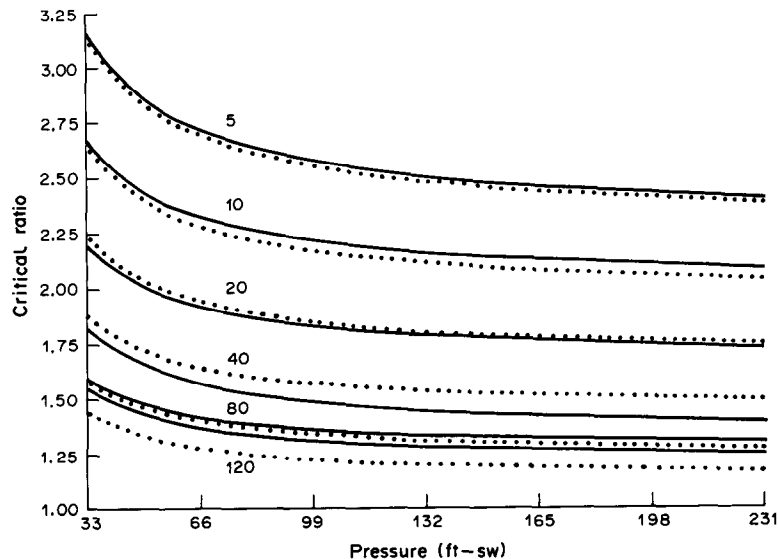


Fig. 3. Fitted and critical ratios.

Table 2. Surfacing ratios and critical N₂ pressures ($P_0 = 33$ ft-sw)

Half-life (min)	Surface ratio	N ₂ pressure (ft-sw)
5	3.15	104
10	2.67	88
20	2.18	72
40	1.76	58
80	1.58	52
120	1.55	51

The tissue curves in Fig. 3 appear hyperbolic-like, roughly parallel functions with surfacing ratios and N₂ pressures as listed in Table 2. The 80 min tissue ratio, 1.58, represents the classical Haldane air value. Faster tissues obviously support higher degrees of supersaturation (and slower tissues lesser degrees) than the Haldane ratio. Considering equations (6) and (8), and the asymptotic behavior of the tissue ratios (Fig. 3), a general form,

$$r = \frac{Ax^B + C}{x + 33}, \quad (18)$$

is suggested for the critical curves. If $B < 1$, $r \rightarrow 0$ as $x \rightarrow \infty$, while $r \rightarrow \infty$, as $x \rightarrow \infty$, for $B > 1$. For $B = 1$, certainly $r \rightarrow A$ when $x \rightarrow \infty$. From Fig. 3, it is doubtful that the tissue curves rise with increasing depth, so that we expect

$$B \leq 1$$

for each tissue curve. Extrapolation of the curves to altitude, $0 \leq P_0 < 33$ ft-sw, depends on both M_0 and P_0 (as discussed later). At the surface, $x = 0$, it follows from equation (18) that

$$r_0 = \frac{C}{33}, \quad (19)$$

so

$$C = M_0, \quad (20)$$

for the M_0 listed in Table 2. The case $B = 1$ yields linearly-dependent N₂ saturation, curves, with corresponding hyperbolic loci of critical ratios, as intimated in other analyses [6, 11, 22] for both air and heliox mixtures.

While a reasonable fit to each of the curves using equation (18) might be expected over depth, a multi-dimensional representation over tissue half-times and depth is desirable. The critical ratios increase with decreasing half-life so, accordingly, equation (18) is extended over half-lives by writing

$$r = \frac{A\tau^D x^B + C\tau^E}{x + 33}, \quad (21)$$

with A, B, C, D and E constants. Other parametric representations are possible, but equation (20) is adequate for our needs. Because the critical ratios increase with decreasing half-life, one expects

$$D < 0, \quad E < 0.$$

The case $D = E$ represents half-life scaling of critical N₂ pressures, anticipated by the apparent parallel behavior of the tissue curves.

The Levenberg–Marquardt algorithm [26], which minimizes the sum of the squares of J non-linear functions in K unknowns, can be employed to fit the data over depth and tissue half-lives. Using the Common Los Alamos Mathematics Software (CLAMS) library routine, SNLSE, to fit the data depicted in Fig. 3, we obtain

$$A = 3.247, \quad B = 0.999, \quad C = 152.770, \quad D = -0.221, \quad E = -0.242, \quad (22)$$

with B, D and E dimensionless and $A\tau^D$ and $C\tau^E$ measured in ft⁻¹ and ft-sw, respectively. Critical

Table 3. Critical tissue ratio limits
($P_0 = 33$ ft-sw)

Half-life (min)	Surface limit	Depth limit
5	3.15	2.27
10	2.67	2.01
20	2.18	1.67
40	1.76	1.34
80	1.58	1.26
120	1.55	1.19

N_2 pressures, M , generated by the fit, satisfy

$$M = A\tau^D x^B + C\tau^E, \quad (23)$$

Figure 3 also plots the fitted critical ratios (\cdots) against the experimental ratios ($—$). Agreement is excellent, with the (fair) exceptions of the 40 and 120 min curves which are off a nominal 10%. With $D \approx E$ and $B = 1$, scaling of the critical pressure curves with $\tau^{0.23}$ is a good overall estimate.

For better agreement with the 40 and 120 min curves, a more general equation of the form

$$M = [(120/\tau)^D + (r/120)^E][Ax^B + C] \quad (24)$$

is useful at the better than 5% level for all six compartments. Using SNLSE, one finds

$$A = 0.590, \quad B = 0.999, \quad C = 24.895, \quad D = 0.37, \quad E = 0.062. \quad (25)$$

As in the previous case the tissue curves scale with τ .

From the above, it is easy to trace the range of ratios by taking the appropriate limits, $x \rightarrow 0$ and $x \rightarrow \infty$. The surfacing values, r_0 , are given in Table 2, and the limiting values at depth, r_∞ , are just the coefficients of x in equations (21) or (24), as discussed earlier. Table 3 lists corresponding limits, (r_0, r_∞) , for the six tissue compartments.

In the U.S. Navy tables [4, 6, 7], as reflected in Fig. 3, critical ratios are larger for faster tissues and greater absolute pressures. As seen in Table 3, the range of variation is not large, especially within compartments. Depending on the method used to extend M -values to reduced pressure (altitude), however, the surface values can change dramatically while the values at depth remain unchanged. Indeed, surfacing (or near-surface) values are the principal concerns in classical decompression applications. Thermodynamic theories [12, 14], however, also focus on values at depth, assuming gas separation from the dissolved (saturated) phase to be a continuous process.

5. ALTITUDE PHENOMENOLOGY

The three-term sum in equation (9) is easily replaced by a single exponential [17] for computational convenience. For small $\gamma_n z$, equation (9) can be expanded to first order, using equation (14), to obtain an effective γ ,

$$\gamma = \sum_{n=1}^3 \alpha_n \gamma_n, \quad (26)$$

so that

$$P_0 = 33 \exp(-\gamma z), \quad (27)$$

and the Cross factors similarly reduce to the expressions,

$$\xi = \exp(\gamma z), \quad (28)$$

with, from equations (10) and (16),

$$\gamma = 0.000038119, \quad (29)$$

in the same units (ft^{-1}). This compact representation of P_0 and ξ , useful in the following, is accurate to 1% at 20,000 ft. At increasing altitude, accuracy is enhanced by the fact that α_{Ar} is small and $\gamma_{N_2} \approx \gamma_{O_2}$. Density differences between fresh and salt water are neglected.

Table 4. Extrapolated intercepts and line slopes below sea level pressure

Half-life (min)	Intercept (ft-sw)	Line slope
5	28.99	2.24
10	23.59	1.92
20	16.73	1.64
40	12.81	1.37
80	11.31	1.21
120	10.98	1.12

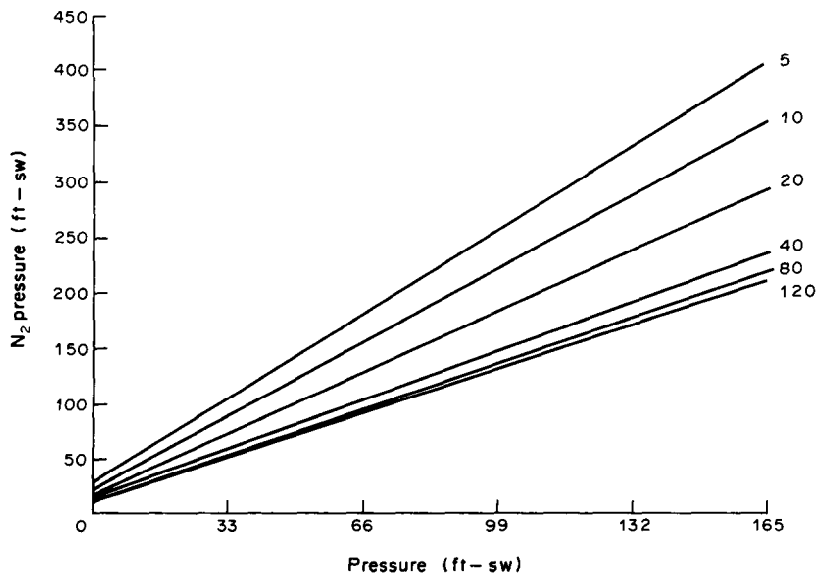
For altitude excursions or flying after diving, projected critical N₂ pressures and ratios are important for table modifications. Two generic extrapolation schemes, which we call the linear pressure [4, 22] and the constant ratio [20, 21, 24] have been proposed for altitude applications. The linear scheme extends the saturation curves in equation (23) to ambient pressures below 33 ft-sw while the constant ratio scheme attempts to maintain the (same) critical ratios of Fig. 3 at altitude. Not as much testing of altitude schedules has transpired, as compared to sea level testing, but the growth of diving has probably given impetus to altitude experiments [19, 22–24].

Since the critical N₂ pressures decrease with absolute pressure, while critical ratios tend to increase, Bell and Borgwardt [22] suggested that the critical N₂ saturation curves might be linearly extended to altitude [negative depth in equation (23)]. The extrapolated, zero pressure intercepts ($x = -33$ ft) and line slopes are positive, and are listed in Table 4. The altitude N₂ curves are just straight line extensions of the tissue curves predicted by equation (23). Corresponding ratios track as hyperbolas at altitude, approach infinity as $P_0 \rightarrow 0$, and therefore suggest greater degrees of relative saturation. The extrapolated critical pressure curves are replotted in terms of absolute pressure (ft-sw) in Fig. 4. Points to the left of 33 ft-sw are the altitude extrapolations, while points to the right recover equation (23). The extrapolation is probably good to near 7000 ft, since atmospheric pressure varies linearly up to that altitude. Beyond that point, atmospheric pressure tends to drop off faster and the linear scheme leads to very large critical ratios.

The severe behavior of the critical ratios as ambient pressure drops in the linear scheme can be mitigated by extending the tissue curves through the origin. One extension, suggested by Smith [20], Cross [21], Wienke [17] and Bassett [24], employs the barometer extrapolation

$$M = C\tau^E \exp(-\gamma z), \quad (30)$$

with $C\tau^E$ the sea level saturation pressures from equation (23), also listed in Table 2. Since absolute

Fig. 4. Critical N₂ pressures (linear extrapolation).

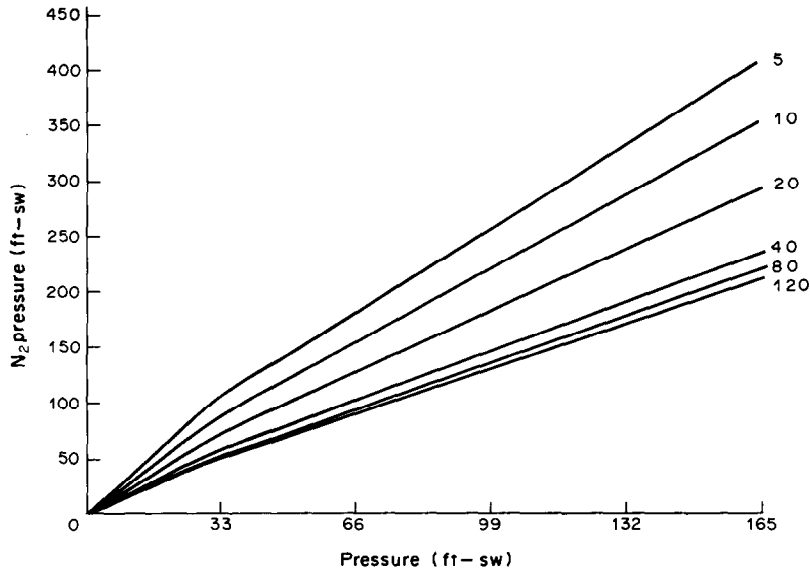


Fig. 5. Critical N_2 pressures (constant ratio extrapolation).

pressure varies in the same proportion, this extension yields constant critical ratios at altitude,

$$r = \frac{C\tau^E}{33}, \quad (31)$$

which are more conservative than the linearly extrapolated ratios. N_2 saturation curves for the constant ratio extrapolation are shown in Fig. 5.

Smith [20] and Cross [21] proposed a constant ratio scheme for altitude diving, based on the equality of ratios for a given altitude exposure and another equivalent exposure at sea level (*similarity* method). Denoting an equivalent sea level depth, d , for excursion to depth, x , at altitude, z , it is easy to determine *similarity* relationships after equating critical ratios:

$$\frac{M(x)}{x + 33\xi^{-1}} = \frac{M(d)}{d + 33}, \quad (32)$$

with ξ given by equation (28). Rearranging the l.h.s. gives the desired form,

$$\frac{\xi M(x)}{\xi x + 33} = \frac{M(d)}{d + 33}, \quad (33)$$

so the transformation is satisfied by

$$d = \xi x \quad (34a)$$

and

$$M(d) = \xi M(x). \quad (34b)$$

Dives at altitude are thus *similar* to deeper excursions at sea level, according to equations (34a, b). Actual stops and ascent rates at altitude, conversely, are slower and shallower [20] by factors of ξ^{-1} . Though the Smith–Cross method is well-known in altitude applications, confusing notions of its extrapolation methodology exist.

6. BULK- OR SINGLE-TISSUE PARAMETERS

While the U.S. Navy adopted the Haldane multi-tissue method just described, the Royal Navy has opted for a single-tissue treatment of N_2 transport. Hempleman [3] introduced the single-tissue concept, but noted that the standard response function, equation (1), so popular in decompression calculations, could not model bounce dive phenomenon with a single parameter exponential term.

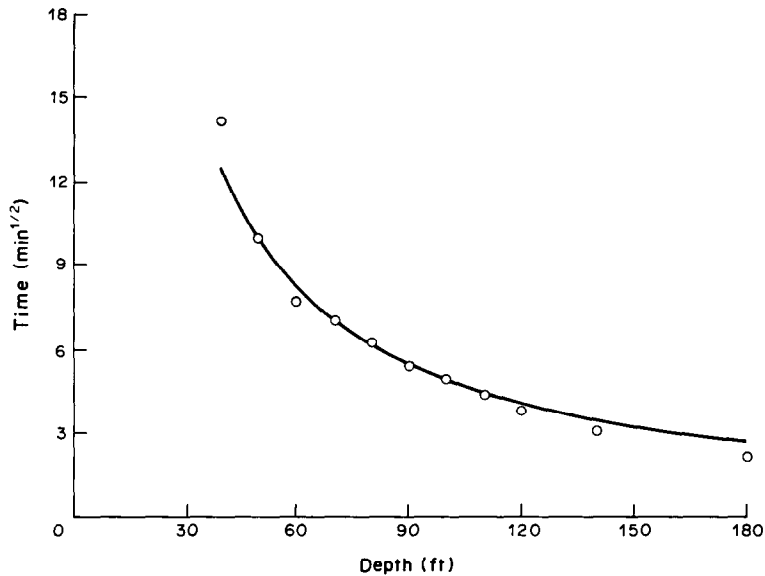


Fig. 6. Predictions of the $t^{1/2}$ law and the no-decompression limits.

Single, no-decompression exposures down to 190 ft satisfy a relatively simple depth–time law [4, 27]:

$$xt^{1/2} = 500 \text{ (ft min}^{1/2}\text{)}, \quad (35)$$

with x (ft) the depth and t (min) the no-decompression time limit. Though the $t^{1/2}$ law provides a good fit for relatively short time intervals, it breaks down for large values of t . Figure 6 compares the predicted $t^{1/2}$ [—, equation (35)] against the no-decompression limits (○) of the tables.

While a single decay parameter, λ , cannot fit the bounce dive data of Fig. 6, a depth-dependent expression [28] can be obtained from equation (3) once a critical ratio is specified. Allowing λ to vary with depth reflects variation in tissue response to pressure, though no physiological coupling is implied. Hempleman [3, 11, 12] also suggested a depth-dependent decompression criteria for the Royal Navy which is a compromise between a fixed pressure and rapidly varying critical ratio,

$$r = \frac{709}{P + 404}, \quad (36)$$

with P given by equation (8). At the surface, $r = 1.62$, while at 100 ft, $r = 1.34$. At approx. 460 ft, $r = 0.79$ and decompression is not possible, which obviously serves to bound the expression.

Bulk models are attractive theoretically since they permit the transfer process to be tracked by one equation. Some feel this type of correlation is more meaningful, because only two constants (M -value and time coefficient) are needed to model the transfer process. With only 2 d.f., a rigorous test of the model is afforded. However, the time constant needed to give a realistic base to the approach implies a diffusion coefficient several orders of magnitude lower than that observed for gases in water or gross tissue. The variable ratio given by equation (36), however, offers a means of coupling, and comparing, the single- and multi-tissue approaches.

Dividing equation (2) by P , equating p/P to equation (36) and simplifying, yields

$$\lambda t = \ln \frac{p_i - P_0}{p_i - rP}, \quad (37)$$

which can be employed to estimate λ from the single, no-decompression time limits (surface bounce). Results are tabulated in Table 5 for various exposures, with $p_0 = 0.79 \times 33 = 26.1$ ft-sw, p_i the continuous N₂ saturation pressures at depth, and $P = P_0 = 33$ ft-sw for immediate return to the surface. One notes that λ is a slowly increasing function of depth with fluctuations.

Since the no-decompression time limits decrease monotonically with depth, while the faster tissue compartments control decompression, in the multi-tissue picture, it is reasonable to expect λ to smoothly increase with depth. Fluctuations can be removed by fitting Table 5 to the logarithmic

Table 5. Decay constants from the no-decompression limits

Depth (ft)	Time limit (min)	Decay constant (min ⁻¹)
40	200	0.0063
50	100	0.0080
60	60	0.0095
70	50	0.0089
80	40	0.0089
90	30	0.0098
100	25	0.0098
110	20	0.0105
120	15	0.0120
140	10	0.0137
190	5	0.0152

expression

$$\lambda = G \ln x + H, \quad (38)$$

with the result

$$G = 0.005217, \quad H = -0.013055, \quad (39)$$

measured as before (min⁻¹).

Comparing the range of equation (38), or Table 5, with equation (5) for the six tissue compartments, it is seen that the depth-dependent predictions of λ overlap the multi-tissue decay parameters for the 120, 80 and 40 min compartments, but not the 20, 10 and 5 min compartments which control deeper exposures in the U.S. Navy tables. Multi-tissue parameters vary by a factor of 24, while the single-tissue parameters only increase by a factor of 3 in the range $40 \leq x \leq 190$ ft, reflecting the compromise between a fixed pressure and rapidly varying decompression ratio, as embodied in equation (36).

Such behavior is neither surprising, nor suspect, since multi-tissue tables omitting the fastest compartments [7, 29] have been fabricated and used in the past. The differences in decay parameters, reflected in the single- and multi-tissue treatments, attest to diversity and granularity in possible computational approaches employed to track critical parameters. The overlaps between the model decay parameters suggest a broad quasi-equivalence between the two approaches.

7. DECOMPRESSION STATISTICS AND THRESHOLD PARAMETERS

Many factors contribute to bends susceptibility. Age, obesity, physical condition, exercise and temperature are a few. Whatever the contributing factors, the distribution of minimum bends depths has been obtained [30] by gradually increasing the pressure, Q , at which a diver has been saturated before rapid decompression to threshold pressure, P . Characterization of the threshold distribution is not only of academic interest, but is also helpful in modifying decompression formats and tolerances, independent of the underlying calculational model.

Hills [31] has determined that the distribution of minimum bends depths fits a Weibull function. If the cumulative fraction of bends cases up to Q is χ , the survivor fraction satisfies the Weibull criterion

$$\ln(1 - \chi) = [(Y - 14.3)/25.1]^{4.73}, \quad (40)$$

with minimum bends differential, Y , measured in ft-sw,

$$Y = Q - P. \quad (41)$$

As the differential grows, the survivor function approaches zero exponentially. The smallest differential for bends provocation is 14.3 ft-sw, which can be contrasted with the average value of 33 ft-sw. The efficiency of the Weibull function in providing an excellent fit to the decompression data is not surprising. The Weibull distribution has been employed heavily in reliability studies involving a multiplicity of fault factors.

In a similar experiment, Hempleman [32] exposed goats to compressed air at absolute pressure, Q , for 12 h and then decompressed the animals to another absolute pressure, P , for several hours, checking for bends development. A few days later, the same goats were exposed to the same pressure, Q , and decompressed to slightly higher, or lower, pressures, P , until a distribution of P was obtained, separating bends from no-bends points. The *titration* is then repeated for a new series of Q . An ensuing linear relationship between Q and P supports the pressure ratio, r , as an index of bends provocation, motivates the linear altitude extrapolation procedure and suggests decreasing critical ratios with depth, simultaneously. This can be seen in the following way.

In analyzing the titration data, Hills [33] proposed a complete separation of bends from no-bends points via the linear (fit) relationship

$$Q = uP + v, \quad (42)$$

with

$$u = 1.72, \quad v = 9.2, \quad (43)$$

and pressures measured in the usual ft-sw. Dividing Q by the ambient pressure, P , separating bends from no-bends occurrences and multiplying Q by 0.79 to convert to N₂ partial pressure, the critical ratios predicted by the titration experiment satisfy

$$r = 0.79 \left(\mu + \frac{v}{P} \right), \quad (44)$$

obviously decreasing with P . At the surface, equation (46) gives $r = 1.62$, while at depth, $r = 1.35$, more in keeping with the range of equation than the range of Table 3. Restricting attention to the slowest three compartments in Table 3, ranges are more comparable, as seen previously in the bulk parameterization of equation (38).

Linear extrapolation of M -values at altitude (absolute pressures below 33 ft-sw) in the multi-tissue scheme is consistent with the titration trend of equation (42). From equation (42), the maximum permissible N₂ pressure, at zero ambient pressure, is approx. 7.3 ft-sw, while the slope of titration curve (in N₂ partial pressure units) is 1.35. Corresponding multi-tissue intercepts and slopes are listed in Table 4. The 120 min intercept, 10.98 ft-sw, and the 40 min slope, 1.37, come closest to the titration curve. However, the corresponding bulk M -value is zero, which is consistent with the constant ratio altitude extrapolation of equation (30). In the absence of extensive altitude decompression data, the difference between the bulk and multi-tissue models is largely academic, especially since the linear and constant ratio extrapolation schemes are equivalent to near 10,000 ft.

8. COMPUTER PROGRAM

DECOMP is a general purpose package [34] which transfers inert N₂ in tissues of arbitrary half-life and contrasts computed N₂ tensions with benchmarked critical (maximum) values used in staged decompression procedures. From the tabulated data used to construct the U.S. Navy tables, linear fits to the critical N₂ pressures are generated, based on the six tissue compartments (5, 10, 20, 40, 80 and 120 min) at sea level, with critical pressure extrapolations to altitude conveniently effected with the fitted barometer equation, which agrees to 1% with mantle pressure measurements.

User inputs include the tissue half-lives dive profiles (depth and time at each level), altitude, ascent (descent) rates, initial tissue pressures and initial depth. For the six compartments (5, 10, 20, 40, 80 and 120 min), the actual saturation data are employed to compute critical pressures and ratios. Between points, saturation curves are interpolated using our fit, which is accurate to 5%. Between levels, N₂ transfer can be estimated by an averaging technique which employs ascent, or descent, rates across levels. Output from DECOMP includes computed N₂ tissue pressures, decompression ratios, critical N₂ tissue pressures, critical decompression ratios and pertinent data at the end of stages (also between stages) for each compartment.

The program is written in FORTRAN for use on Crays, CDC 7600s, CDC Cybers or any other machine with at least 420000 byte high-speed storage and a FORTRAN compiler. The program is 200 card images long. DISSPLA graphics software [35] is convenient for post-processing, but not required for calculations. Terminal, printer and graphics server are the only necessary

peripherals to process I/O. Calculations for six compartments in a 10-level excursion require < 1 s on the Cray.

DECOMP models gas transfer, according to the foregoing multi-tissue analysis, in divers breathing compressed air (79% N₂ and 21% O₂). Repetitive and multi-level (depth and time) activities are traced continuously in time. Computed N₂ pressures are compared with critical values used to fabricate the U.S. Navy air tables. In repetitive applications, continuous tensions at the end of one stage form the initial values for the following stage. The tissue equations used to transfer N₂ treat compartments as uniform media of differing half-lives as discussed earlier.

9. SUMMARY

An extension parameterization of critical N₂ pressures and decompression ratios, at sea level and altitude, in both single- and multi-tissue models, has been described. The information is useful for rapid numerical application, extrapolation, and interpolation within the constraints of the air tables and associated methodology. Fits to the data included critical N₂ pressures and critical ratios for the multi-tissue U.S. Navy approach, the single-tissue decay constants for bounce applications in the Royal Navy scheme, and ambient air pressures and Cross factors at altitude. The phenomenology of decompression at sea level and altitude was discussed, and an exponential altitude extrapolation of critical pressures and ratios was also suggested. Pertinent statistics and implications were presented and discussed. Consistency between the multi-tissue and bulk models was described, and numerical correlations with experiment were identified and contrasted. A software package, DECOMP, incorporating the elements of this analysis has been constructed and is available to interested users.

These types of calculational methods, in the absence of complete physical information, can only address a limited range of conditions. No model approach yet is purely synthetic, relying upon first principles and handbook constants. This analysis suggests nothing so new, but rather summarizes and encapsulates a vast body of experimental data into a manageable set of parametric equations which are motivated both by traditional and recent developments. Even as more comprehensive theories develop, bodies of experimental data, such as described, must still be integrated into workable hypotheses.

REFERENCES

1. A. E. Boycott, G. C. C. Damant and J. S. Haldane, *J. Hyg. (Lond.)* **8**, 342 (1908).
2. A. R. Behnke, *Nav. med. Bull.* **35**, 219 (1937).
3. H. V. Hempleman, RN Medical Research Committee Report UPS 131 (1952).
4. M. Des Granges, USN Experimental Diving Unit Research Report 5-57, Washington, D.C. (1957).
5. O. E. Van Der Aue, R. J. Kellar, E. S. Brinton, G. Barron, H. D. Gilliam and R. J. Jones, USN Experimental Diving Unit Research Report 1-51, Washington, D.C. (1951).
6. R. D. Workman, USN Experimental Diving Unit Research Report 6-65, Washington, D.C. (1965).
7. J. V. Dwyer, USN Experimental Diving Unit Research Report 1-57, Washington, D.C. (1956).
8. A. Fick *Ann In Phys.* **170**, 59 (1855).
9. J. S. Haldane and J. G. Priestly, *Respiration*. Yale Univ. Press, New Haven Conn. (1922).
10. J. B. Bateman, *Decompression Sickness*. Saunders, Baltimore, Md (1951).
11. P. B. Bennett and D. H. Elliott, *The Physiology and Medicine of Diving and Compressed Air Work*. Williams & Wilkins, Baltimore, Md (1982).
12. B. A. Hills, *Decompression Sickness*. Wiley, New York (1977).
13. *United States Naval Diving Manual, NAVSHIPS 0 994-001-9010*. U.S. Government Printing Office, Washington, D.C. (1970).
14. B. A. Hills, *A Thermodynamic and Kinetic Approach to Decompression Sickness*. Library Board South Australia, Adelaide (1966).
15. F. W. Sears, *Thermodynamics*. Addison-Wesley, Reading, Mass (1953).
16. R. G. Fleagle and J. A. Businger, *Atmospheric Physics*. Academic Press, New York (1963).
17. B. R. Wienke, *Ascent Lines* **5**, 4 (1976); *ibid.* **1**, 12 (1984).
18. A. R. Bennke, *Milit. Surg.* **90**, 9 (1942).
19. P. O. Edell, J. J. Carroll, R. W. Honaker and E. L. Beckman, *Aerospace Med.* **40**, 1105 (1969).
20. C. L. Smith, *Altitude Procedures for the Ocean Diver*. NAUI Technical Publication 5. National Association of Underwater Instructors, Montclair, (1975).
21. E. R. Cross, *Skin Diver Mag.* **16**, 49 (1967); *ibid.* **19**, 17 (1970).
22. R. L. Bell and R. E. Borgwardt, *Undersea biomed. Res.* **3**, 1 (1976).
23. M. R. Boni, R. Schibli, P. Nussberger and A. A. Buhlman, *Undersea biomed. Res.* **3**, 189 (1976).
24. B. E. Bassett, *Proc. 11th Int. Conf. Underwater Ed.* **1**, 41 (1979); *Sport Diver Mag.* **1**, 23 (1980).

25. *U.S. Standard Atmospheres 1966*. U.S. Government Printing Office, Washington, D.C. (1962).
26. J. J. More, *Numerical Analysis. Lecture Notes In Mathematics*, No. 630. Springer-Verlag, Berlin (1977).
27. G. J. Duffner, J. F. Synder and L. L. Smith, USN Experimental Diving Unit Research Report 3-59, Washington, D.C. (1959).
28. B. R. Wienke, *Ind. J. Technol.* **15**, 326 (1977).
29. O. D. Yarbrough and A. R. Behnke, *J. ind. Hyg. Toxicol* **21**, 213 (1937).
30. W. E. Crocker, F. C. Goodenough and W. M. Davidson, RN Medical Research Committee Report UPS 118, London (1951).
31. B. A. Hills, *Int. J. Biomet.* **12**, 343 (1968).
32. H. V. Hempleman RN Medical Research Committee Report UPS 168, London (1957).
33. B. A. Hills, *Rev. Subaqua Physiol. Hyperb. Med.* **1**, 249 (1968).
34. B. R. Wienke, *Comput. Phys. Commun.* **40**, 327 (1986).
35. *DISSPLA: Display Integrated Software System and Plotting Language*. Integrated Software Systems Corp., San Diego, Calif. (1980).